#### Renewable Energy 101 (2017) 376-386

Contents lists available at ScienceDirect

**Renewable Energy** 

journal homepage: www.elsevier.com/locate/renene

## Investigation of the incoming wind vector for improved wind turbine yaw-adjustment under different atmospheric and wind farm conditions

# G. Cortina <sup>a, \*</sup>, V. Sharma <sup>b</sup>, M. Calaf <sup>a</sup>

<sup>a</sup> Department of Mechanical Engineering, University of Utah, Utah, USA
<sup>b</sup> School of Architecture, Civil and Environmental Engineering, EPFL, Lausanne, Switzerland

#### ARTICLE INFO

Article history: Received 23 November 2015 Received in revised form 31 May 2016 Accepted 5 August 2016

Keywords: Large eddy simulation LIDAR Wind energy Wind farm Wind turbines Yaw-misalignment

## ABSTRACT

Regardless of the evolution of wind energy harvesting, the way in which turbines obtain in-situ meteorological information remains the same - i.e. using traditional wind vanes and cup anemometers installed at the turbine's nacelle, right behind the blades. As a result, misalignment with the mean wind vector is common and energy losses up to 4.6% can be experienced as well as increases in loading and structural fatigue. A solution for the near-blade monitoring is to install wind LIDAR devices on the turbines' nacelle. This technique is currently under development as an alternative to traditional in-situ wind anemometry because it can measure the wind vector at substantial distances upwind. But at what upwind distance should they interrogate the atmosphere? and, what is the optimal average time in which to learn about the incoming flow conditions? This work simulates wind fields approaching isolated wind turbines and wind turbine arrays within large wind farms using Large Eddy Simulations. The goal is to investigate the existence of an optimal upstream scanning distance and average time for wind turbines to measure the incoming wind conditions under different ambient atmospheric conditions. Results reveal no significant differences when measuring the incoming wind vector at different upstream distances, regardless of the atmospheric stratification. Within this framework a 30 min readjustment period is observed to perform the best.

© 2016 Elsevier Ltd. All rights reserved.

### 1. Introduction

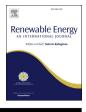
Over the past ten years wind energy harvesting has experienced a rapid growth, with an overall installed global power average annual increase of the total installed wind power capacity of 25% per year in the last ten years (2002–2012) [1]. Throughout this time wind turbine designs have evolved, with increases in rotor diameter and overall efficiency designs. By 2004–08 most wind turbines had a ~70–80 meter rotor diameter, and currently, rotor diameter designs are approaching 100 m with an average hub height of 80 m [2]. Engineering improvements have accompanied the development of large rotors. However, the way in which wind turbines obtain in-situ meteorological information remains the same – traditional wind vanes and cup anemometers are installed at the

\* Corresponding author. *E-mail address*: gerard.cortina@utah.edu (G. Cortina). *URL*: http://wet.mech.utah.edu/ turbines nacelle, right behind the blades. The orientation and other operating parameters of the turbine are governed by these two wind measurements through the use of a control loop [3].

These wind measurements have important drawbacks, especially with increasing rotor diameters. Since the velocity is measured at a single point immediately behind the blades, turbine misalignment with the mean wind direction is common [4]. In principle, this problem should be overcome using the so-called nacelle transfer functions (NTFs), which describe the relation between the nacelle wind vector measurements and the unperturbed wind vector upstream of the wind farm. The NTFs are used to properly correct nacelle measurements [5]; however, they have a strong variability from site to site and they don't account for changes in atmospheric-stratification. For example, Vanderwende and Lundquist [6] experimentally showed distinct wind turbine performances, with respect to a given wind turbine power coefficient curve, under different atmospheric regimes. They demonstrated under-performance during stably-stratified periods and over-performance during unstably-stratified periods and







377

moderate wind speeds  $(8-12 m s^{-1})$ . An additional drawback from the near-blade monitoring is the limited time it provides the wind turbine controllers to adjust the turbine operating parameters' to account for changes in the approaching wind flow [7]. This latency in adjusting to ambient wind direction and speed subjects the blades and turbine structure to unanticipated wind gusts or extreme incoming wind conditions. These velocity aberrations induce increased loading, structural fatigue, power-train failures and associated increases in maintenance costs. A solution is to install forward directed wind Laser Imaging Detection and Ranging (LIDAR) on the turbines' nacelles. Future studies might find a way to measure ahead of time these velocity aberrations and wind gusts with the use of wind LIDARs, which together with advanced control systems will advice the wind turbine controls system to correct their settings. Also experimental LES studies should be performed in order to study the turbulent flow upstream of the wind turbines. Although LIDAR technology has been around since the early 1970s [8–10], it hasn't been until the recent advancements in optical fiber technology that such LIDARs have become affordable. Because wind LIDARs measure the frequency shift of the backscattered light initially sent by a laser beam, making it possible to measure the along-beam component of the wind velocity at various distances upwind of the rotor. By using a cone-scanning or volumetric scanning technique, the full three-dimensional wind components can be used to measure the approaching unperturbed winds [7, 11 - 171.

Further, recent studies have shown the potential of optimizing the overall power output of a wind farm by forcing a fixed vawmisalignement on the upwind wind turbine arrays such that their corresponding wakes are laterally deviated and reducing their corresponding interaction with the downstream turbines [17–19]. Gebraad et al. [18] developed a control-oriented dynamic model that determines the best orientation of a given wind turbine to avoid turbine-wake interaction. Also the National Renewable Energy Laboratory (NREL) experimentally implemented at the Fishermens Atlantic City Windfarm a control strategy to reduce the wind-turbine wake interaction, obtaining up to a 10% increase in harvested power for the overall wind farm [19]. Yet, for these wind farm optimization techniques to be efficient, it is critical to accurately know the correct yaw-alignment of the turbine with respect to the incoming wind vector. The use of a wind LIDAR mounted on the turbine's nacelle has been shown to provide good yaw alignment and better power curves than traditional wind vanes, therefore enhancing the overall power output [20–22]. However, wind LIDAR systems are optimized to measure over a fixed upwind range and average over a certain period of time. The question remains as to what upwind distance they should interrogate the atmosphere and for what time period. In the present work, different upstream scanning distances and averaging times are evaluated within different atmospheric stratifications using Large Eddy Simulations (LES) driven with the experimental data of the well known Cooperative Atmospheric Surface Exchange Study (CASES-99) [23-25]. In Section 2, the LES code is presented in detail together with the sub-grid model, the boundary conditions and the wind turbine model used. Section 3 introduces the study cases considered, and Section 4 introduces the numerical results, first with respect to different upstream scanning distances and second with respect to distinct yawing averaging times. Finally, the conclusions are presented in Section 5.

#### 2. Large-eddy simulation framework

The present work uses the Large Eddy Simulation code introduced in Sharma et al. [26]. The numerical code integrates the nondimensional, incompressible, and filtered Navier-Stokes (NS) equations together with the continuity equation. The NS equation is implemented using its rotational form to assure conservation of energy and mass of the inertial terms [27]. The effect of temperature is introduced by means of a buoyancy term in the NS equation, which is the result of the Boussinesq approximation, and which is obtained from solving a coupled advection-diffusion equation for the potential temperature ( $\theta$ ). Therefore, the full set of equations solved is,

$$\frac{\partial \tilde{u}_i}{\partial x_i} = 0, \tag{1}$$

$$\frac{\partial \tilde{u}_i}{\partial t} + \tilde{u}_j \left( \frac{\partial \tilde{u}_i}{\partial x_j} - \frac{\partial \tilde{u}_j}{\partial x_i} \right) = -\frac{1}{\rho} \frac{\partial p^*}{\partial x_i} - \frac{\partial \tilde{\tau}_{ij}}{\partial x_j} + g \left( \frac{\tilde{\theta} - \langle \tilde{\theta} \rangle}{\theta_0} \right) \delta_{i3} + f(\tilde{u}_2 - v_C) \delta_{i1} - f(\tilde{u}_1 - u_C) \delta_{i2} + f_i$$
(2)

$$\frac{\partial\tilde{\theta}}{\partial t} + \tilde{u}_j \frac{\partial\tilde{\theta}}{\partial x_j} = -\frac{\partial\pi_j}{\partial x_j}.$$
(3)

Here, the tilde () represents the LES filtering operation at the grid-size  $\Delta$ , and the angle brackets ( $\langle \cdot \rangle$ ) represent a horizontal average, with index notation used to specify rectangular Cartesian coordinates i = 1,2,3 = x,y,z. The reference temperature is denoted by  $\theta_0$ . The  $\tilde{\tau}_{ij}$  term represents the deviatoric part of the momentum sub-grid stress (SGS) term, which is modeled using the Lagrangian Scale Dependent model of Bou-Zeid et al. [28], and  $\pi_j$  represents the sub-grid component of the thermal equation, which is correspondingly modeled with the adaptation of the Lagrangian Scale Dependent model for scalars introduced in Calaf et al. [29]. The modified kinematic pressure term ( $p^*$ ) includes the filtered pressure term ( $p^*$ )

sure term and the trace of the SGS tensor  $\left(\tilde{p}/\rho + \tilde{\tau}_{kk}/3 + \frac{1}{2}\tilde{u}_{j}\tilde{u}_{j}\right)$ .

Within this work, the flow is forced with a time- and heightindependent geostrophic wind  $(u_G, v_G)$ , where f represents the Coriolis parameter, and  $\delta_{ii}$  is the Kronecker delta ( $\delta_{ii} = 1$ , if i = j, and 0 otherwise). The  $f_i$  term represents the sink of momentum induced by the wind turbine. It is represented as a body force (per unit volume) and it is modeled using the traditional actuator-disk with rotation (ADR, see Wu et al. [30]) including the dynamical yawalignement of Sharma et al. [26]. Note that within the formulation of these equations the potential temperature is an active scalar that modifies the momentum equation by means of the buoyancy term, which accounts for the vertical motions induced by the thermal stratification. Further, as it is traditional in LES of atmospheric flows, the viscous effects are neglected and the flow is therefore characterized by a very large Reynolds number. The numerical discretization of the equations follows the one introduced by Moeng [31] and Alberston et al. [32], where a pseudo-spectral approach with a staggered-grid is used. Therefore, second-order finite differences are used in the vertical direction and a spectral discretization using the Fast Fourier Transform in the West (FFTW) [33] library is implemented in the horizontal directions. As a result of the Fourier discretization in the horizontal directions the numerical domain becomes periodic, eliminating the need for lateral boundary conditions and becoming infinite in practical effects.

The equations are dealiazed using the 3/2-rule [34], and timeintegrated using a second order Adam-Bashfort scheme. The numerical algorithm is fully parallelized using the Message-Passing Interface (MPI) with a total of 64 processors and the pressure solver is further parallelized with the pipeline Thomas algorithm [35]. As a result of the periodic boundary conditions in the horizontal directions, there is no need for lateral boundary conditions. For the top boundary a zero-flux and zero-shear are imposed, with Download English Version:

https://daneshyari.com/en/article/4926891

Download Persian Version:

https://daneshyari.com/article/4926891

Daneshyari.com